EXPERIMENTAL STUDY ON BUCKLING BEHAVIOR OF GFRP ANGLE SECTIONS

Japan Steel Tower Co., Ltd. Regular Member ○ Doni Suprapto, Yuki Ito
Japan Steel Tower Co., Ltd. Non-Member Makoto Honda

1. Introduction

Equal-angle steel is generally used as truss members in steel towers. Recently, problems such as corrosion due to deterioration over time have become apparent, and the use of GFRP with excellent corrosion resistance has been studied. However, studies have been conducted mainly on cross-sectional shapes such as I- and C-shapes, while equal-angle shape have not been studied much [1)2)3)].

Therefore, this paper discusses the basic behavior and buckling strength of the GFRP angle sections using the experimental buckling and FEM analysis method.

2. Specimen and Experimental Method

The specimens are set as an equal-leg angle section with dimensions of 50 mm × 6 mm (hereafter referred to as B series) and 75 mm × 6 mm (hereafter referred to as C series). According to JIS standards, material property tests are carried out to obtain relevant properties. The details of the specimens and material properties are shown in Table1. Fig. 1 shows the experimental configuration. The specimen was set in 3000kN test machine and placed between pin-pin supports JIG. A JIG set of pin support capable of releasing rotation about the minor axis of the angle section (v- v axis direction) was used.

Table1. Detail of specimen & Material properties

No.	Geometry b (mm)	t (mm)	b/t	r_u (mm)	r_v (mm)	λ	Total Case
B-4	50	6	8.3	19.2	9.8	40	3
B-7						70	3
B-10						100	3
B-13						130	3
B-16						160	3
B-19						190	3
C-4	75	6	12.5	29.4	14.8	40	3
C-7						70	3
C-10						100	3
C-16						160	3
C-19						190	3

E_L	E_T	G_{LT}	ν_{LT}	ν_{TL}
GPa	GPa	GPa		
26.6	9.15	3.18	0.256	0.085

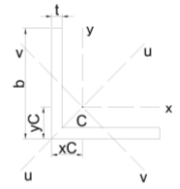

Fig.1 Experimental configuration

3. Results and Discussions

3.1 Experimental Results

The experimental buckling loads (P_{exp}) and modes of failure are shown in Table 2 along with the theoretical value (P_{pred}). The buckling modes of the experimental results show good agreement with the prediction buckling modes. The buckling modes can be classified by a combination of flexural-torsional (flexure about the major axis and torsion about the shear center) and pure flexural (flexure about the minor principal axis) as shown in Fig. 2. Each specimen with λ ratio of 40~70 buckled in flexural-torsional, λ=100~130 buckled in transitions from flexural-torsional to flexural, and λ=160~190 buckled in pure flexural buckling. From the experimental results, the flexural buckling mode occurred under rotation around the weak axis (v-v axis). Therefore, the buckling strength can be estimated using Euler's equation about the weak axis. Meanwhile, in the flexural-torsional buckling mode, buckling strength is estimated by flexural buckling about the major axis (u-u axis) and torsional buckling about the longitudinal axis. This is because the GFRP material used in this experiment has a much lower shear modulus than the longitudinal modulus (E_L/G_{LT} = 8.3). The theoretical value (P_{pred}) of the Euler's buckling load[4)] and flexural-torsional buckling load[5)] that is assumed from the buckling behavior can be calculated by the following equations:

$$P_{fv}=\frac{\pi^2 E_L}{(K_v L_v/r_v)^2}A_g \quad (1)$$

$$P_{ft}=\frac{P_{fu}+P_{tz}}{2H}\left[1-\sqrt{1-\frac{4HP_{fu}P_{tz}}{(P_{fu}+P_{tz})^2}}\right] \quad (2)$$

In which

$$P_{fu}=\frac{\pi^2 E_L}{(K_u L_u/r_u)^2}A_g \quad (3)$$

$$P_{tz}=\left[\frac{G_{LT}}{(b/t)^2}+\frac{\pi^2 E_L}{12(1-V_{LT}V_{TL})(K_Z L_Z/t)^2}\right]A_g \quad (4)$$

In the above equations, P_{fv}, P_{fu}, P_{tz}, P_{ft} denote flexural buckling load about the v-axis (minor axis), flexural buckling about the u-axis (major axis), torsional buckling about the longitudinal axis, and flexural-torsional buckling, respectively. K_vL_v and K_uL_u are the effective lengths for bending about the principal axes v and u. K_zL_z is the effective length for twisting about the longitudinal axis, Ag is the gross sectional area approximated as $2bt$, and H parameter is defined as $5/8$.

Table 2 Buckling load and modes

No.	P_{exp} 1 (kN)	2 (kN)	3 (kN)	AVG (kN)	P_{pred} K_v=1 (kN)	K_v=0.7 (kN)	Eqn.	$\frac{P_{exp}}{P_{pred}}$ K_v=1	K_v=0.7	Buckling Modes exp 1	2	3	pred
B-4	43.68	54.63	50.37	49.56	38.44	-	P_{ft}	1.29	-	FTB	FTB	FTB	FTB
B-7	37.14	38.31	38.61	38.02	28.41	-		1.34	-	FTB-C	FTB-C	FTB	FTB
B-10	31.29	24.54	28.71	28.18	15.75	32.14	P_{fv}	1.79	0.88	FTB	FTB	FB	FB/FTB
B-13	20.16	17.97	18.90	19.01	9.32	19.02		2.04	1.00	FB	FB	FB	FB
B-16	12.18	10.74	14.97	12.63	6.15	12.55		2.05	1.01	FB	FB	FB	FB
B-19	6.87	10.74	6.90	8.17	4.36	8.90		1.87	0.92	FB	FB	FB	FB
C-4	32.25	35.58	33.45	33.76	26.09	-	P_{ft}	1.29	-	FTB-C	FTB	FTB	FTB
C-7	27.72	26.94	27.93	27.53	20.10	-		1.37	-	FTB	FTB	FTB	FTB
C-10	24.15	24.54	24.51	24.40	23.62	-	P_{fv}	1.03	-	FTB	FB	FTB	FB/FTB
C-16	10.98	9.69	8.91	9.86	9.22	-		1.07	-	FB	FB	FB	FB
C-19	6.54	6.78	6.69	6.67	6.54	-		1.02	-	FB	FB	FB	FB

F: Flexure, T: Torsional, C: Crush

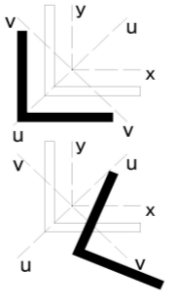

Fig.2 Buckling modes FB and FTB

At the time of the experiment, the movement of the bottom pin JIG of the test machine was poor. Hence, the pin support cannot be fully reproduced on the B series with a range λ of 100~190. As shown in Table 2, the buckling load (P_{exp}) of the B series is 1.79~2.05 times higher than the theoretical value (P_{pred}). In the B series, it is probable that the end-restraints became nearly pin-fix end restraints, and as a result, the effective buckling lengths (K_vL_v) were shortened. Due to this circumstance, K_v was corrected to 0.7. It can be seen that the P_{pred} are generally consistent with the experimental results. Especially on P_{ft}, most of the ratios

Keywords: GFRP, angle sections, buckling behavior
Contact address: 1-7-1 Kitahama, Wakamatsu-ku, Kitakyushu-shi, Fukuoka, Japan, 〒 808-0023 Tel: +81- 93-751-5313

are larger than 1, indicating that the equation is conservative. Fig. 3 presents the graph value of the B and C series compiled with the theoretical value. It is illustrated that flexural buckling controls the behavior of buckling modes when λ exceeds χ and P smaller than *FTB Limit*. This observed behavior can be represented through the following equations for χ and *FTB Limit*:

$$\chi \approx \left(\frac{5}{8}\frac{b^2}{t}\sqrt{\frac{E_L}{G_{LT}}}\right)/r_v \quad (5)$$

$$FTB\ Limit = \frac{G_{LT}}{(b/t)^2}A_g 0.9 \quad (6)$$

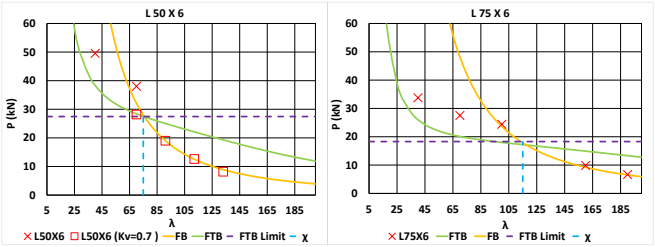

Fig.3 Relation between P and λ in B & C series

3.2 FEM Analysis

In order to validate the experimental results, FEM analysis was performed with FE models modeled using 3D hexahedral solid elements using FEMAP with NX Nastran. Advanced Nonlinear Solver (SOL 601) is used to consider large deformations and nonlinearity of the material. The material properties of the FE model are listed in Table 1. The FE model simulated all aspects of the experimental conditions. Initial geometric imperfections determined based on the results of buckling modes were considered in this FE model. There are two models of initial geometry imperfection as shown in Fig. 4, initial bow for flexure mode (*FB*) and initial twist for flexure-torsional mode (*FTB*). The imperfections were defined as half sinusoidal wave function over the member length (L) with an amplitude of *L/1000*. To validate the phenomena on the B series, as mentioned before, the boundary condition on models were set into pin-fix end restraints as shown in Fig. 4. It is observed that the FEM analysis are good in correspondence with the experimental results. Table 3 shows the comparison of P_{exp} and P_{FEM} computed by the analysis. Fig. 5 shows the buckled mode shape of FE models and experimental results.

Table.3 P_{exp} and P_{FEM}

No.	P_{exp}				P_{FEM}		$\frac{P_{exp}}{P_{FEM}}$	
	1	2	3	AVG	P-P	P-F	P-P	P-F
	kN	kN	kN	kN	kN	kN		
B-4	43.68	54.63	50.37	49.56	50.00	-	0.99	-
B-7	37.14	38.31	38.61	38.02	30.00	-	1.27	-
B-10	31.29	24.54	28.71	28.18	13.50	27.30	2.09	1.03
B-13	20.16	17.97	18.90	19.01	8.00	16.50	2.38	1.15
B-16	12.18	10.74	14.97	12.63	5.38	11.07	2.35	1.14
B-19	6.87	10.74	6.90	8.17	3.88	7.98	2.11	1.02
C-4	32.25	35.58	33.45	33.76	34.50	-	0.98	-
C-7	27.72	26.94	27.93	27.53	25.00	-	1.10	-
C-10	24.15	24.54	24.51	24.40	20.94	-	1.17	-
C-16	10.98	9.69	8.91	9.86	8.38	-	1.18	-
C-19	6.54	6.78	6.69	6.67	6.00	-	1.11	-

P-P: PIN-PIN, P-F: PIN-FIX,

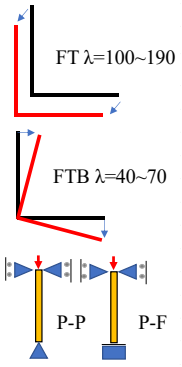

Fig.4 Initial geometric imperfection & restraints condition of FE model

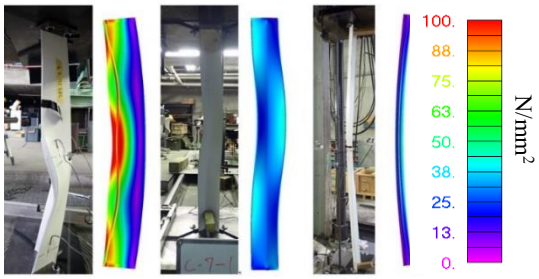

Fig.5 Buckling mode shape validation
(Scale indicate von-misses contour, left to the right λ=40,70, 160 C series)

4. Conclusions

Based on the results of the study, the following conclusions are made:

- Specimens with λ range of 40~70 failed by flexure-torsional buckling, λ range of 100~130 failed by either flexure-torsional buckling or flexure buckling, and λ range of 130~190 failed by pure flexure buckling.
- Global buckling formula (Euler) was successfully used for predicting the buckling load of intermediate and long specimens. The theoretical equation of P_{ft} also provides a good estimate for short specimens that needed to consider the combination of torsional and flexure buckling load.
- It is observed that in small slenderness specimens (λ=40~70), an increase in the ratio of *b/t* from 8.3 (50 mm × 6 mm) to 12.5 (75 mm × 6 mm) decreased the buckling load by about 30%.
- Flexure-torsional buckling becomes the main failure on small and intermediate slenderness because the GFRP material used in this experiment has a much lower shear modulus than the longitudinal modulus (high ratio of E_L/G_{LT}).
- Finite element models were developed and validated against the experimental results. The FEM analysis with initial geometry imperfection models predicted well the buckling load and failure modes.

References

1) Monteiro, A.C.L, Malite, M.: Behavior and design of concentric and eccentrically loaded pultruded GFRP angle columns. Thin-Walled Struct., 161, 2021, 107428.
2) Cardoso, D.C.T, Togashi, B.S: Experimental investigation on the flexural-torsional buckling behavior of pultruded GFRP angle Columns, Thin-Walled Struct., 125, 2018, 269-280.
3) Sirajudeen, R.S, Sekar, R.: Buckling Analysis of Pultruded Glass Fiber Reinforced Polymer (GFRP) Angle Sections. Polymer, 12(2532), 2020.
4) 土木学会：複合構造標準示方書　原則編・設計編, 2014.
5) Zureick, A., Steffen, R.: Behavior and design of concentrically loaded pultruded angle struts. J. Struct. Eng. N. Y., 126(3), 2000, 406–416.